ACADEMIC PRESS

Available online at www.sciencedirect.com
SCIENCE DIRECT®

Journal of Catalysis 215 (2003) 108–115

JOURNAL OF CATALYSIS

www.elsevier.com/locate/jcat

Bulk structure and catalytic properties of mixed Mo–V–Sb–Nb oxides for selective propane oxidation to acrylic acid

Jamal N. Al-Saeedi,[a] Vadim V. Guliants,[a,*] Olga Guerrero-Pérez,[b] and Miguel A. Bañares [b]

[a] *Department of Chemical Engineering, University of Cincinnati, Cincinnati, OH 45221-0171, USA*
[b] *Instituto de Catalisis y Petroleoquimica, CSIC, E-28049 Madrid, Spain*

Received 3 September 2002; revised 26 November 2002; accepted 26 November 2002

Abstract

The bulk mixed Mo–V–Sb–Nb–O catalysts, which are a candidate catalytic system for the selective oxidation of propane to acrylic acid, were investigated to elucidate the bulk structure and catalytic behavior of these complex materials. These mixed oxides were prepared via a redox reaction between V^{5+} and Sb^{3+} in the presence of Mo^{6+} and Nb^{5+} and characterized by potentiometric titrations, XRD, Raman spectroscopy, electron microscopy (TEM), and bulk elemental analysis. A potentiometric titration method was used to determine concentrations of metal cations in various oxidation states. XRD and Raman spectroscopy identified $Mo_6V_9O_{40}$, MoO_3, $SbVO_4$, and a Nb-stabilized defect phase of a V-rich molybdate as the major phases present. Electron microscopy illustrated the heterogeneity of the bulk oxide phases present in the model Mo–V–Sb–Nb–O system on the submicron scale. MoO_3 comprised the bulk of this mixed metal oxide system, while the surface region of these model catalysts contained mixed Mo–V–Sb–Nb oxides. The rutile $SbVO_4$ phase was inefficient in propane oxidation to acrylic acid, while mixed Mo–V–Nb oxides were capable of producing acrylic acid at ∼ 20 mol% yield.
© 2003 Elsevier Science (USA). All rights reserved.

Keywords: Mo–V–Sb–Nb mixed-oxide catalysts; Bulk structure; Selective oxidation of propane; Structure–activity relationships

1. Introduction

The availability and low cost of alkanes have generated much recent interest in the oxidative catalytic conversion of alkanes to olefins, oxygenates, and nitriles in the petroleum and petrochemical industries [1–4]. Direct selective oxidation of lower alkanes is highly attractive because it would bypass the energy intensive endothermic steam cracking or dehydrogenation reactions currently employed to manufacture olefin intermediates from natural gas and petroleum feedstocks for subsequent oxidation. It also presents a possibility of replacing the currently used raw materials, mostly olefins and aromatics, with more environmentally friendly alkane substrates.

The oxidative catalytic conversion of propane to propylene and oxygenates (acrolein and acrylic acid) is most efficient over vanadia-based catalysts [2,5–7]. BP is currently developing a process based on a V–Sb–O mixed oxide catalyst [8–12], while the Mitsubishi and Rohm and Haas efforts are focused on a Mo–V–Nb–Te mixed oxide catalyst [3,13–15]. Toagosei reported bulk mixed Mo–V–Sb–Nb–O system [16], which displayed selectivity for propane oxidation to acrylic acid of ∼ 30 mol% at ∼ 31 mol% propane conversion at 400 °C. Despite the promise of the results obtained, very limited fundamental information was reported about the synthesis, solid-state chemistry, and catalytic properties of this mixed metal oxide system. This information is critical for the development of improved catalysts for selective oxidation of propane [17,18].

We investigated in this study the role of synthesis parameters such as Mo addition sequence, Mo/V and Sb/V ratios, on solution, and solid-state chemistries of the model Mo–V–Sb–Nb–O system in an effort to provide detailed structure–activity/selectivity relationships for this promising catalytic system for selective propane oxidation. We report the major crystalline phases found in the mixed Mo–V–Sb–Nb oxide catalysts and characterized by XRD, Raman spectroscopy, and electron microscopy for different compositions of these mixed oxide catalysts. Kinetic studies of propane oxidation over these model catalysts shed new light on the nature of the

* Corresponding author.
E-mail address: vadim.guliants@uc.edu (V.V. Guliants).

0021-9517/03/$ – see front matter © 2003 Elsevier Science (USA). All rights reserved.
doi:10.1016/S0021-9517(02)00186-0

active and selective phases for propane oxidation to acrylic acid.

2. Experimental

2.1. Catalyst preparation

The mixed Mo–V–Sb–Nb oxides were prepared in an aqueous medium using ammonium metavanadate, NH_4VO_3 (Aldrich, 99+%), antimony trioxide, Sb_2O_3 (99+%, Aldrich), ammonium heptamolybdate (81–83 wt% as MoO_3, Alfa Aesar), oxalic acid (98 wt%, Aldrich), and hydrated niobium oxide (80.3 wt% Nb, Reference Metals Company). Niobium oxalate was synthesized by reacting oxalic acid with hydrated niobium oxide in an aqueous medium under stirring at 80 °C. The slurry was heated under stirring until a clear solution was obtained. The solution was evaporated to dryness in air at 80 °C to yield $Nb_2(C_2O_4)_5 \cdot xH_2O/C_2H_2O_4$.

Two synthesis routes were followed in the preparation of mixed Mo–V–Sb–Nb oxides. The first preparation route (a) involved the redox reaction between aqueous V^{5+} and Sb^{3+} under reflux conditions at 120 °C for 12 h [16–18], cooling the solution to 80 °C, followed by addition of the Mo^{6+} and niobium oxalate solutions. The entire synthesis was conducted under a bubbling oxygen atmosphere. The resulting solution was evaporated to dryness and calcined for 4 h at 600 °C under N_2. This synthesis was carried out for compositions 1a and 2a (Table 1).

The second route (b) involved the redox reaction between the aqueous V^{5+} and Sb^{3+} in the presence of Mo^{6+} at 80 °C followed by the addition of the niobium oxalate solution. Again, the synthesis was conducted under bubbling oxygen. The resulting solution was evaporated to dryness and calcined for 4 h at 600 °C under N_2. This synthesis route was followed for compositions 1b, 2b, 3, and 4 (Table 1). These compositions corresponded to the best performing catalysts reported in the patent literature [16] and were employed here to study the effects of Mo addition, Mo/V and Sb/V ratios on solution, and solid-state chemistries of the model Mo–V–Sb–Nb–O system.

2.2. Physicochemical characterization

2.2.1. Potentiometric titration

The distribution of various oxidation states (V^{3+}, V^{4+}, V^{5+}, Sb^{3+}, Sb^{5+}, Mo^{5+}, and Mo^{6+}) during synthesis was determined by potentiometric titration and gravimetric techniques. The potentiometric titration technique consisted of a series of titrations with $KMnO_4$ (0.01 N) and $(NH_4)_2Fe(SO_4)_2$ (0.01 N) solutions shown in Fig. 1.

Table 1
Synthesis compositions of mixed Mo–V–Sb–Nb oxide system

Sample	V/Mo	Sb/Mo	Nb/Mo
1a, 1b	0.3	0.25	0.1
2a, 2b	0.3	0.1	0.1
3	0.3	0	0.1
4	1.0	1.0	0.1

The potentiometric titration was carried out employing solutions containing 3–4 μmoles of the metal ions. The sample solution was diluted with deionized water to a total volume of 400 ml and divided into two 200-ml aliquots, solution A and solution B. Solution A was titrated with Fe^{2+} to determine the concentration of V^{5+} ions. The endpoint indicative of V^{5+} mole number was found by plotting the derivative of the potential with respect to the number of moles of Fe^{2+} added. Solution B was first titrated with $KMnO_4$ and the potential of the redox electrode was plotted against the amount of $KMnO_4$ added. The moles of $KMnO_4$ added at the endpoint corresponded to the number of moles of V^{4+} and V^{3+}. Solution C, obtained after $KMnO_4$ titration, was titrated with Fe^{2+} to determine the combined concentration of V^{5+}, V^{4+}, and V^{3+} ions. This titration technique was validated using reference compounds of V ($NH_4V^{5+}O_3$, $V^{4+}OSO_4$, and $V^{3+}Cl_3$). The experimental error of the potentiometric titration technique was ∼ 1–2 mol%.

Although $KMnO_4$ was capable of oxidizing Mo^{5+} and Sb^{3+} under synthesis conditions employed in this study, these species were not present in solutions upon completion of the redox reactions. Oxygen bubbled through synthesis solution easily oxidized Mo^{5+} and maintained it in the Mo^{6+} oxidation state. On the other hand, the Sb^{3+} species are insoluble and may be determined gravimetrically. However, due to the low Sb/V ratios employed in synthesis (Table 1), all Sb_2O_3 was oxidized into the soluble Sb^{5+} species.

2.2.2. Powder XRD

Powder XRD patterns were recorded on a Siemens D-500 diffractometer using a Cu-K_α radiation source with a peak intensity reproducibility of ±3%. Crystalline phases were quantified by XRD using the elemental Si standard (33 wt% Si in a mixture with model oxide catalysts, peak intensities referenced to the $2\theta = 28.6°$ Si peak).

2.2.3. Raman spectroscopy

Raman spectra were collected using a single monochromator Renishaw System 1000 equipped with a thermoelectrically cooled CCD detector (−73 °C) and holographic super-Notch filter. The holographic Notch filter removes the elastic scattering more completely than in the case of a triple monochromator spectrometer, which results in a Raman signal enhancement. The samples were excited with the 514-nm Ar line. The spectral resolution and spectrum acquisition time were ca. 3 cm^{-1} and 300 s, respectively. The spectra were obtained under dehydrated conditions (ca. 390 K) in a hot stage (Linkam TS-1500) in a flow of dry air. The spectra of hydrated samples (not shown) were obtained at room temperature in a flow of humid air.

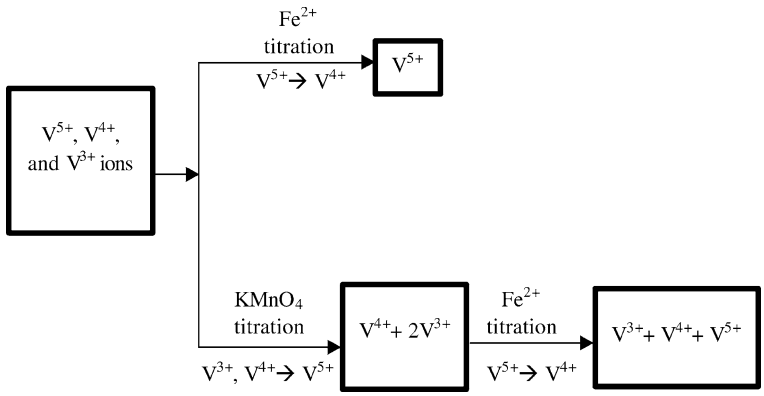

Fig. 1. Potentiometric titration of Mo–V–Sb–Nb–O synthesis solutions.

2.2.4. Electron microscopy

The microstructural characterization of the model Mo–V–Sb–Nb–O catalysts was conducted using a JOEL-2010 transmission electron microscope. This unit was equipped with an energy dispersive spectrometer (EDS) for the local elemental analysis of solid samples.

2.2.5. Kinetic studies of model Mo–V–Sb–Nb–O system

Kinetic studies were conducted at 400 °C using a feed of 4.4 vol% propane, 7.0 vol% oxygen, 62.4 vol% steam (balance nitrogen) at a flow rate of 30 cm^3/min (GHSV of 1800 h^{-1}). Reactions were carried out with 1.0 cm^3 of catalysts in a 3/8-in diameter stainless steel tubular microreactor placed in a programmable oven. An HP 5890II gas chromatograph equipped with an FID and TCD was employed for the reaction product analysis. The carbon balances agreed within 5 mol%. The BET surface areas were measured using a Micromeritics TriStar 3000 porosimeter.

3. Results and discussion

3.1. Redox reactions during catalyst synthesis

Two synthesis routes to the mixed Mo–V–Sb–Nb oxides were investigated. The first route involved the redox reaction between V^{5+} and Sb^{3+} under ∼ 12 h of reflux at 120 °C, followed by Mo^{6+} and Nb^{5+} addition under bubbling oxygen. The proposed redox reactions in solution are shown below.

$$V^{5+} + Sb^{3+} \rightarrow V^{3+} + Sb^{5+}, \quad \text{(a)}$$

$$V^{5+} + V^{3+} \rightarrow 2V^{4+}, \quad \text{(b)}$$

$$Mo^{6+} + V^{4+} \rightarrow Mo^{5+} + V^{5+}, \quad \text{(c)}$$

$$Mo^{6+} + V^{3+} \rightarrow Mo^{5+} + V^{4+}, \quad \text{(d)}$$

$$4Mo^{5+} + O_2 \rightarrow 4Mo^{6+} + 2O^{2-} \text{ (under bubbling } O_2\text{)}. \quad \text{(e)}$$

The reactions (a) and (b) occurred simultaneously under reflux conditions at 120 °C for 12 h. Molybdenum was added after cooling the combined V/Sb solution to 80 °C and maintained in the Mo^{6+} state by bubbling oxygen through the synthesis solutions. This was confirmed by studying individual redox reactions employing separate pairs of ions appearing in reactions (a)–(e). These studies indicated that reaction (a) was much slower than reaction (b), which in turn was somewhat slower than reactions (c) and (d), suggesting that the resulting solution contained V^{4+} and V^{5+} as the major V species. As mentioned earlier, for the Sb/V ratios ($\leqslant 1.0$) employed in synthesis, Sb^{5+} was the dominant oxidation state for the Sb species in solution.

In the second synthesis route, the redox reaction between V^{5+} and Sb^{3+} occurred at 80 °C in the presence of Mo^{6+} and Nb^{5+} under bubbling oxygen conditions. The redox reactions (a)–(e) occurred simultaneously at 80 °C when V^{5+}, Sb^{3+}, and Mo^{6+} were present in solution. The final synthesis solution was expected to contain V^{5+} and V^{4+} as the major V species. Sb^{5+} and Mo^{6+} were expected to be the dominant solution species for Sb and Mo during synthesis.

3.2. Potentiometric titration

To obtain insights into the redox processes during catalyst synthesis for the two synthesis routes, it is important to determine the oxidation states of V ions (V^{3+}, V^{4+}, and V^{5+}) in the mixed oxide solutions upon completion of redox reactions. This information is also required to study relationships between the distribution of various oxidation states in synthesis solution and the formation of various oxidized and partially reduced mixed metal oxide phases in solid catalysts possessing distinct catalytic behavior in propane oxidation to acrylic acid. The schematic of the potentiometric titration method for the mixed Mo–V–Sb–Nb oxides is shown in Fig. 1. The distribution of the V oxidation states (V^{3+}, V^{4+}, and V^{5+}) was determined by three independent potentiometric titrations described in the experimental section. The total V content (Table 2) determined by these titrations agreed well with the amount of V employed in synthesis. Mo cations in the synthesis solution were expected to be in the +6 state because O_2 bubbled during synthesis rapidly oxidized Mo^{5+} according to reaction (e). This was confirmed by a potentiometric

Table 2
Oxidation state distribution in the synthesis solutions (mol%)

Sample	V^{5+}	V^{4+}	V^{3+}	Total V balance[a] (%)
1a	86.7	12.0	1.3	2.1
1b	51.4	47.3	1.4	3.2
2a	78.6	21.4	0.0	0.8
2b	63.6	34.1	2.3	1.7
3	100.0	0.0	0.0	1.2
4	78.8	21.2	0.0	4.2

[a] Total V balance = (the moles of V in the synthesis solution − the moles of V determined by potentiometric titrations)/(the moles of V in the synthesis solution) × 100.

titration of a reference Mo^{5+} solution, which was almost instantaneously oxidized to Mo^{6+} under bubbling oxygen at 80 °C. All Sb was in the Sb^{5+} state at the end of synthesis. This was determined gravimetrically due to the insolubility of Sb^{3+} oxide species in water.

The oxidation state distribution of the metal oxide species in solution was determined immediately after completion of redox reactions (Table 2). Sample numbers shown in Table 2 correspond to compositions shown in Table 1. The synthesis solutions for catalysts 1a and 1b had the same composition. However, for compositions 1a and 2a, Mo^{6+} was added after the redox reaction between V^{5+} and Sb^{3+}, was completed. For compositions 1b, 2b, 3, and 4, Mo^{6+} was added simultaneously with Sb^{3+} to the aqueous V^{5+} solution. Potentiometric titration showed that the order of Mo addition during synthesis affected V oxidation states in solution. Mo^{6+} addition simultaneously with Sb^{3+} to the aqueous V^{5+} solution always led to a noticeable increase in the V^{4+} concentration (Table 2). In the case of composition 3, which contained no Sb (Table 1), all vanadium was in the +5 oxidation state.

3.3. Solid-state chemistry of Mo–V–Sb–Nb–O system

3.3.1. Powder XRD

The identification of crystalline phases was carried out by comparing the experimental XRD patterns with those reported in the JCPDS files: MoO_3 (76-1003), $Mo_6V_9O_{40}$ (19-0813), $SbVO_4$ (16-0600), Sb_2MoO_6 (25-0107), and $3MoO_2 \cdot Nb_2O_5$ (18-0840). Also, a number of reference phases were obtained and characterized by XRD: MoO_3, V_2O_5, Sb_2O_4, $Mo_6V_9O_{40}$, $Mo_{0.61–0.77}V_{0.31–0.19}Nb_{0.08–0.04}O_x$ (the defect Mo–V–Nb–O phase [7]), $3MoO_2 \cdot Nb_2O_5$, and $SbVO_4$. The reference $Mo_6V_9O_{40}$ phase and the defect Mo–V–Nb–O phase with the $Mo_{0.70}V_{0.22}Nb_{0.08}$ composition were synthesized according to the reported synthesis procedures [7,10,17,18]. Although the XRD patterns of these phases are similar, $Mo_6V_9O_{40}$ may be distinguished from the defect Mo–V–Nb–O phase by the presence of reflections at 39.2° and 49.6°. Commercially available phases such as Sb_2O_3 (99+%, Aldrich), Sb_2O_5 (99.999%, Alfa Aesar), and Nb_2O_5 (80.3 wt% Nb, Reference Metals Company) were obtained and characterized as well.

The XRD patterns shown in Fig. 2 revealed that the phase composition of assynthesized mixed Mo–V–Sb–Nb oxides depended on both the synthesis composition and the synthesis route. All mixed oxides contained MoO_3, $Mo_6V_9O_{40}$, defect Mo–V–Nb–O phase, and $SbVO_4$ (for Sb-containing samples). The peak at 2θ of 27.2° in Fig. 2 corresponded to a mixture of phases: $Mo_6V_9O_{40}$, defect Mo–V–Nb–O, MoO_3, and $SbVO_4$. Several weak reflections were observed at 2θ of 22.2°, 23.1°, 31.2°, and 47.7°, which were tentatively assigned to the $3MoO_2 \cdot Nb_2O_5$ phase. The presence of this phase was further confirmed in the Mo–V–Sb–Nb oxide system after these model catalysts were

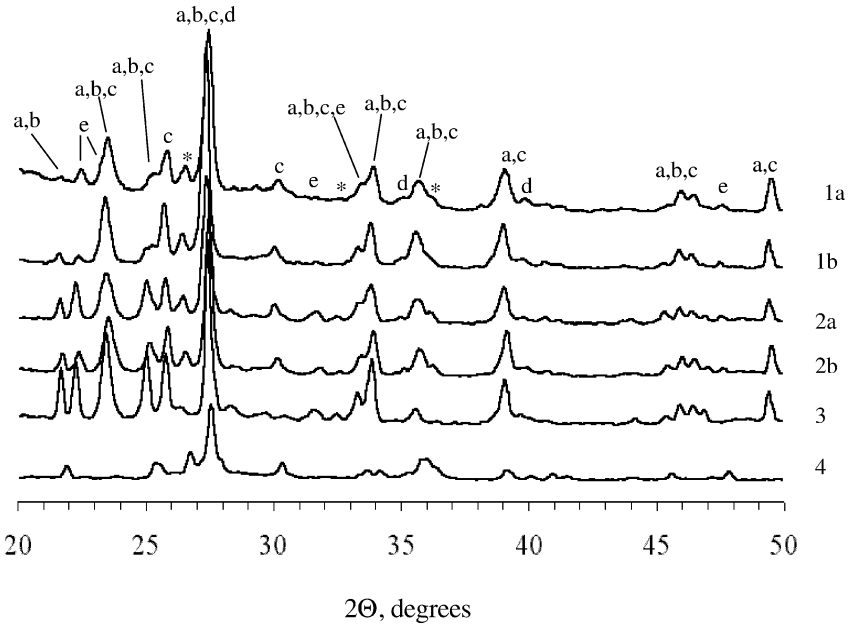

Fig. 2. XRD patterns of mixed Mo–V–Sb–Nb systems (a, $Mo_6V_9O_{40}$; b, $Mo_{0.6–0.71}V_{0.31–0.19}Nb_{0.08–0.04}O$; c, MoO_3; d, $SbVO_4$; e, $3MoO_2 \cdot Nb_2O_5$; *, unassigned).

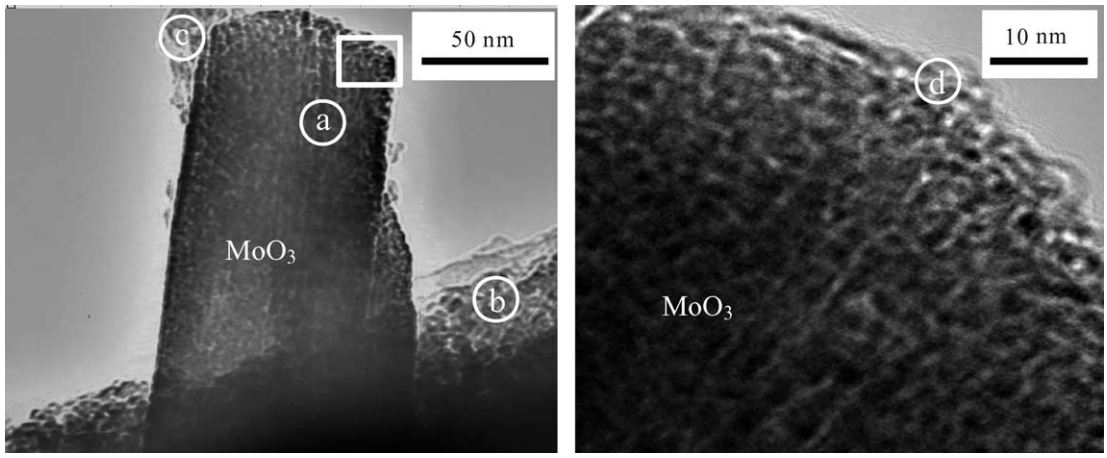

Fig. 3. TEM images of the $Mo_1V_{0.3}Sb_{0.25}Nb_{0.1}$ catalyst (composition 1a). The image to the right shows a high-resolution TEM of the square area of the left image. EDS elemental composition: spot a (23 at% Mo and 77 at% O), spot b (20 at% Mo, 3 at% V, 2 at% Sb, 13 at% Nb and 62 at% O), spot c (24 at% Mo, 8 at% V, 5 at% Sb, 16 at% Nb and 47 at% O), and spot d (4 at% Mo, 38 at% V, 28 at% Sb, and 30 at% O).

Table 3
The combined $Mo_6V_9O_{40}/Mo_{0.6–0.71}V_{0.31–0.19}Nb_{0.08–0.04}O$ phase content in model Mo–V–Sb–Nb–O catalysts, wt%

Crystalline phase	Composition (wt%)					
	1a	1b	2a	2b	3	4
$Mo_6V_9O_{40}$/Mo–V–Nb	12.8	30.7	14.7	34.6	23.4	5.2

calcined at 700 °C that resulted in enhanced crystallization of the $3MoO_2 \cdot Nb_2O_5$ phase [10]. Other unassigned weak reflections were also observed at 2θ 26.6°, 32.3°, and 36.2°.

The combined content of the $Mo_6V_9O_{40}$ and the defect Mo–V–Nb–O phases was determined using Si as a reference (Table 3). We estimated the content of the $Mo_6V_9O_{40}$/Mo–V–Nb–O phases by subtracting MoO_3 content from the combined content of $MoO_3/Mo_6V_9O_{40}$/Mo–V–Nb–O phases identified by the 2θ reflections at 23.5°, 33.9°, and 35.7°. The content of $Mo_6V_9O_{40}$/Mo–V–Nb–O phases was affected by the synthesis composition and the synthesis route. The content of these phases was enhanced in the case of samples with V/Mo = 0.3, Sb/V = 0.4, and Mo addition along with Sb during synthesis (synthesis route b shown in Table 3). The high content of these phases was observed for solutions with a high V^{4+} concentration at the end of synthesis.

3.3.2. Electron microscopy

The morphology of the model Mo–V–Sb–Nb oxides was dominated by the presence of rod-like MoO_3 crystals. TEM confirmed the presence of 5–20-nm nanocrystals of the $Mo_6V_9O_{40}$ and defect Mo–V–Nb–O phases attached to the surface of large (∼ 200-nm) MoO_3 crystals. Typical morphology of the mixed Mo–V–Sb–Nb oxide 1a near the surface region is shown in Fig. 3. V, Sb, and Nb species were found predominantly in the surface region of the MoO_3 rods. The bulk compositions for different particle morphologies observed in the mixed Mo–V–Sb–Nb oxide system were determined by EDS. The crystalline rod shown in Fig. 3 had a composition of 23 at% Mo and 77 at% O, which corresponded to MoO_3. The encircled areas shown in Fig. 3 displayed compositions corresponding to a mixture of phases: $Mo_6V_9O_{40}$, defect Mo–V–Nb–O, and $SbVO_4$.

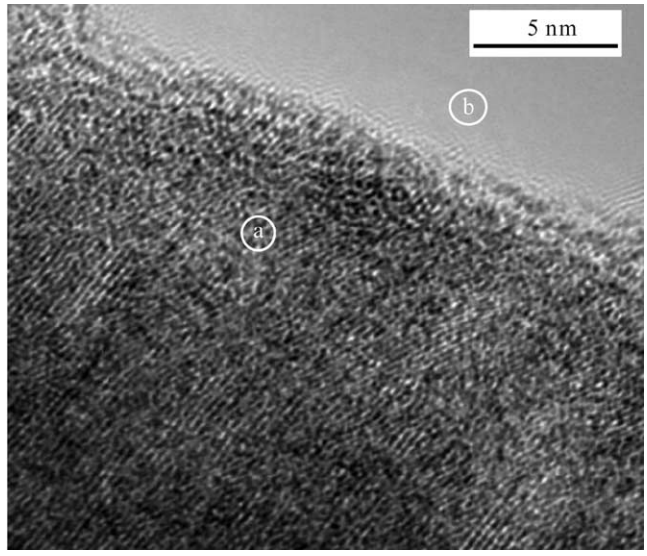

Fig. 4. High-resolution TEM image of the $Mo_1V_{0.3}Sb_{0.25}Nb_{0.1}$ catalyst (composition 1a). EDS elemental composition: spot a (36 at% Mo, 11 at% V, 4 at% Nb, and 49 at% O) and spot b (26 at% Mo, 7 at% V, 8 at% Sb, 5 at% Nb, and 54 at% O).

To further investigate the microstructure of these mixed oxides, we carried out a high-resolution TEM study of the model Mo–V–Sb–Nb–O catalyst 1a (Fig. 4). The particular location shown in Fig. 4 corresponded to the defect Mo–V–Nb–O phase, which has a layered structure with a 4.0-Å d-spacing and the following composition: 36 at% Mo, 11 at% V, 4 at% Nb, and 49 at% O. This composition corresponded to the reported defect Mo–V–Nb–O phase [7]. The surface region had a composition of 26 at% Mo, 7 at% V, 8 at% Sb, 5 at% Nb, and 54 at% O, which again corresponded to a mixture of phases.

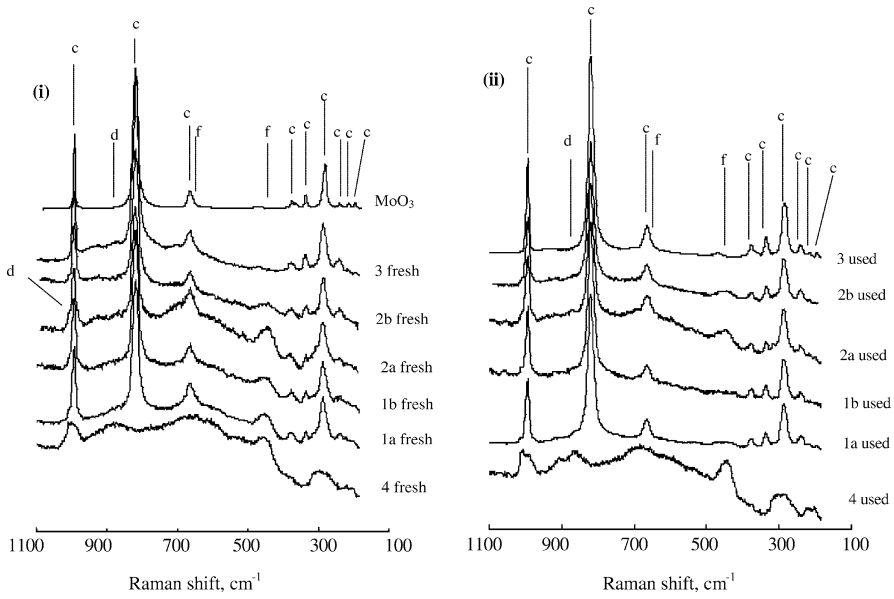

Fig. 5. Raman spectra of dehydrated mixed Mo–V–Sb–Nb oxide catalysts (c, MoO_3; d, $SbVO_4$; f, Mo–Sb–O): (i) fresh and (ii) used. The Raman spectrum of MoO_3 is shown in (A) for comparison.

3.3.3. Raman spectroscopy

The Raman spectra of the fresh and dehydrated used Mo–V–Sb–Nb–O catalysts are shown in Fig. 5. The Raman spectra of hydrated samples did not show any changes with respect to the dehydrated samples. The spectra of the Mo-rich catalysts (compositions 1a, 1b, 2a, 2b, and 3) were dominated by the Raman bands at 993, 818, 664, 376, 364, 335, 232, 241, 214, 196, 152, and 126 cm^{-1} that corresponded to the α-MoO_3 phase (Fig. 5). For composition 4 ($Mo_1V_1Sb_1Nb_{0.1}$), no Raman bands of α-MoO_3 were observed in agreement with the XRD data (Fig. 2). Weak bands near 880 and 1020 cm^{-1} in the Raman spectrum of composition 4 were characteristic of the rutile $SbVO_4$ phase (Guerrero-Pérez et al., in preparation).

The Raman band around 880 cm^{-1} was very weak in the spectra of catalysts 1a and 2a. However, the Raman band of $SbVO_4$ at 1020 cm^{-1}, which was insensitive to the degree of catalyst hydration, appeared as a shoulder in the Raman spectra of these catalysts. In these samples, Sb and V species were allowed to interact prior to the addition of Mo during the preparation of these catalysts. The spectrum of catalyst 4 exhibited additional weak Raman bands at 300, 450 cm^{-1}, and a broad band centered around 650 cm^{-1}. These Raman bands were probably due to some Mo–Sb–O phase, because these Raman features were absent in the spectrum of catalyst 3, which contained no Sb.

Therefore, the model Mo–V–Sb–Nb–O catalysts prepared via the synthesis route (b) appeared to contain not only $SbVO_4$, but also some other mixed antimonate phase(s). This synthesis route also resulted in a greater extent of V^{5+} reduction and Sb^{3+} oxidation. Since Sb^{5+} is more reactive than Sb^{3+}, it may combine more readily with Mo and particularly V to form Sb-containing mixed metal oxide phases, such as the rutile $SbVO_4$ phase, where Sb^{5+} and V^{3+} have been detected in the bulk by the Mössbauer and EPR spectroscopies, respectively [19,20]. The reference $3MoO_2 \cdot Nb_2O_5$ phase exhibited intense Raman bands at 996, 865, 758, 675, and 243 cm^{-1} (not shown here), which were not observed in any of the model Mo–V–Sb–Nb–O catalysts. Therefore, the Raman evidence along with the XRD data suggest that the $3MoO_2 \cdot Nb_2O_5$ phase was not fully developed in the model Mo–V–Sb–Nb oxide catalyst due to the low activation temperature used in the present study.

3.4. Kinetic studies

The study of catalyst composition 1a was reported in the patent literature [16]. This catalyst was studied at 350–450 °C (Fig. 6) and exhibited the selectivity to acrylic acid of 33 mol% and propane conversion of 37 mol% at 410 °C. The reaction was run under conditions where the diffusional limitations could be neglected. The propane conversion and the selectivity to acrylic acid at 400 °C for the six model catalysts are shown in Table 4. It is evident that the order of Mo addition is important for catalytic activity and selectivity. For the synthesis routes employed in this study, catalysts 1b and 2b demonstrated a higher activity and selectivity to acrylic acid than catalysts 1a and 2a, respectively. This can be explained by the higher combined content of the $Mo_6V_9O_{40}$/Mo–V–Nb phases in catalysts 1b and 2b. The catalysts with different Sb/V ratios (1a vs 2a and 1b vs 2b) showed no significant differences in either the propane conversion or the selectivity to acrylic acid. This indicated that Sb did not affect the catalytic properties for the Sb/V ratios in the 0.4–1.0 range.

The study of the catalyst with composition 3 demonstrated that Sb is not directly involved in the critical steps of propane oxidation to acrylic acid. This catalyst contained

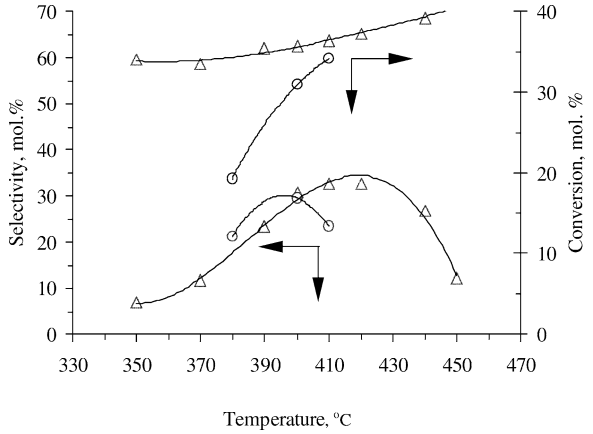

Fig. 6. Selectivity–conversion data for propane oxidation to acrylic acid over mixed Mo–V–Sb–Nb oxides: (△) $Mo_1V_{0.3}Sb_{0.25}Nb_{0.1}$ (composition 1a of this study) and (○) Takahashi et al. [16] (feed: 4.4 vol% propane, 7.0 vol% oxygen, 62.4 vol% steam and balance nitrogen. GHSV = 1800 h^{-1}).

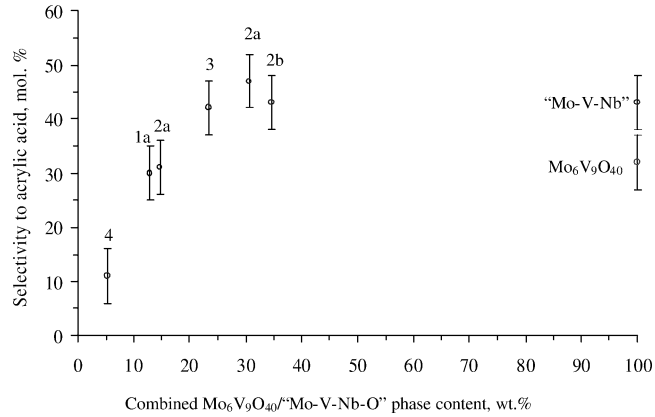

Fig. 7. Selectivity to acrylic acid for propane oxidation over the mixed Mo–V–Sb–Nb oxides and reference phases as a function of combined $Mo_6V_9O_{40}$/Mo–V–Nb–O phase content (feed: 4.4 vol% propane, 7.0 vol% oxygen, 62.4 vol% steam and balance nitrogen. Temp. = 400 °C. GHSV = 1800 h^{-1}).

no Sb and afforded acrylic acid yields comparable to those observed for catalysts 1b and 2b. This was further confirmed by the results of kinetic studies of the reference defect Mo–V–Nb–O phase, which displayed similar catalytic properties to those of composition 3. Low synthesis Mo/V ratios (composition 4) resulted in a decrease of catalytic activity and the selectivity to acrylic acid. Kinetic studies of the relevant reference phases, namely $SbVO_4$, $3MoO_2 \cdot Nb_2O_5$, $Mo_6V_9O_{40}$, and defect Mo–V–Nb–O, were conducted under the same reaction conditions. Only the $Mo_6V_9O_{40}$ and defect Mo–V–Nb–O phases showed high yields of acrylic acid, while no acrylic acid was produced over the reference $SbVO_4$ and $3MoO_2 \cdot Nb_2O_5$ phases (Table 4). In addition, catalysts 1a and 2a, which contained some $SbVO_4$, were much less efficient for the acrylic acid formation. The selectivity to acrylic acid correlated with the content of the $Mo_6V_9O_{40}$ and defect Mo–V–Nb–O phases in the model Mo–V–Sb–Nb–O system (Fig. 7). The yield of acrylic acid over pure $Mo_6V_9O_{40}$ and Mo–V–Nb–O phases was comparable to the yields obtained over the mixed Mo–V–Sb–Nb oxides shown in Table 4.

4. Conclusions

The phase composition of the mixed Mo–V–Sb–Nb oxide system strongly depended on the synthesis route and composition. The two synthesis routes used in this study resulted in a mixture of phases: $Mo_6V_9O_{40}$, MoO_3, rutile $SbVO_4$, and the defect Mo–V–Nb–O. In this four-component mixed metal oxide system, Mo addition sequence during synthesis was important for achieving enhanced catalytic activity and selectivity in propane oxidation to acrylic acid. The addition of Mo simultaneously to the Sb and V precursors prevented the formation of the $SbVO_4$ phase, which was unselective for this propane oxidation reaction. The kinetic and physicochemical characterization studies indicated that the $Mo_6V_9O_{40}$ and defect Mo–V–Nb–O phases are the likely active and selective phases in propane oxidation to acrylic acid. The $Mo_6V_9O_{40}$ and defect Mo–V–Nb–O phases displayed a high yield of acrylic acid, while the rutile $SbVO_4$ phase and $3MoO_2 \cdot Nb_2O_5$ were unselective.

Table 4
Propane oxidation over model Mo–V–Sb–Nb–O catalysts

Catalyst/phase	BET area (m^2/g)	Conversion (mol%)	Selectivity to propylene (mol%)	Selectivity to acrylic acid (mol%)	Yield of acrylic acid (mol%)
1a	5.0	35	2	30	10
1b	8.1	38	11	47	18
2a	3.8	34	2	31	11
2b	3.6	39	7	43	17
3	2.7	40	5	42	17
4	6.4	28	2	11	3
$Mo_6V_9O_{40}$	9.8	36	20	32	12
Mo–V–Nb–O	3.6	42	8	39	16
Rutile $SbVO_4$	55.1	58	16	∼0	∼0
$3MoO_2 \cdot Nb_2O_5$	1.6	42	4.3	∼0	∼0

Acknowledgments

The authors thank the University of Cincinnati Faculty Development Council for financial support and Dr. Robert Ference (Reference Metals Company) for the gift of Nb oxalate. Miguel A. Bañares acknowledges funding from CICYT, Spain (IN96-0053), for the acquisition of the Raman system. Jamal N. Al-Saeedi acknowledges the Public Authority for Applied Education, Kuwait, and Olga Guerrero-Pérez acknowledges the Ministry of Science and Technology, Spain, for their PhD fellowships.

References

[1] F. Cavani, F. Trifiró, Catal. Today 51 (1999) 561.
[2] M.M. Bettahar, G. Costentin, L. Savary, J. Lavalley, Appl. Catal. A 145 (1996) 1.
[3] M.M. Lin, Appl. Catal. A 207 (2001) 1.
[4] P. Concepción, J.M. López Nieto, J. Pérez-Pariente, J. Mol. Catal. A: Chem. 99 (1995) 173.
[5] R. Catani, G. Centi, F. Trifiró, R.K. Grasselli, Ind. Eng. Chem. Res. 31 (1992) 107.
[6] US Patents 4746641, 1988; 4784979, 1988; 4788317, 1988; 4871706, 1989; 4877764, 1989; 4879264, 1989; assigned to the Standard Oil Company, Ohio.
[7] E.M. Thorsteinson, T.P. Wilson, F.G. Young, P.H. Kasai, J. Catal. 52 (1978) 116.
[8] G. Centi, S. Perathoner, F. Trifiró, Appl. Catal. A 157 (1997) 143.
[9] L. Brazdil, A.M. Ebner, J.F. Brazdil, J. Catal. 163 (1996) 117.
[10] K. Ruth, R. Burch, R. Kieffer, J. Catal. 175 (1998) 27.
[11] R.K. Grasselli, Catal. Today 49 (2000) 141.
[12] H. Zanthoff, S. Schaefer, G. Wolf, Appl. Catal. A 164 (1997) 105.
[13] J.F. Brazdil, A.M. Ebner, F. Cavalcanti, Appl. Catal. A 165 (1997) 51.
[14] T.C. Watling, G. Deo, K. Seshan, I.E. Wachs, J.A. Lercher, Catal. Today 28 (1996) 139.
[15] A. Corma, J.M. López Nieto, G. Kremenic, J.L.G. Fierro, Appl. Catal. A 61 (1990) 235.
[16] M. Takahashi, X. Tu, T. Hirose, M. Ishii, US Patent 5994580, assigned to Toagosei Co. Ltd., Japan, 1999.
[17] S.A. Holmes, J.N. Al-Saeedi, V.V. Guliants, P. Boolchand, D. Georgiev, U. Hackler, E. Sobkow, Catal. Today 67 (2001) 403.
[18] J.N. Al-Saeedi, V.V. Guliants, Appl. Catal. A 237 (2002) 111.
[19] T. Birchall, A.W. Sleight, Inorg. Chem. 15 (4) (1976) 868.
[20] F.J. Berry, M.E. Brett, Inorg. Chim. Acta 7 (1983) L205.